Journal of Inflammation Research

Dovepress
Taylor & Francis Group

Open Access Full Text Article

ORIGINAL RESEARCH

Proteomic Profiling of Serum-Derived Exosomes in Oral Lichen Planus: FN1-C3-ECM Crosstalk as a Potential Novel Therapeutic Target

Xue-Ying Wang[1,*], Yu-Fang Deng[1,2,*], Sheng-Jin Xue[1], Wei-Qun Guan[1]

[1]Department of Stomatology, Union Hospital, Fujian Medical University, Fuzhou, Fujian Province, 350001, People's Republic of China; [2]School of Stomatology, Fujian Medical University, Fuzhou, Fujian Province, 350004, People's Republic of China

*These authors contributed equally to this work

Correspondence: Wei-Qun Guan, Department of Stomatology, Union Hospital, Fujian Medical University, No. 29 of Xinquan Road, Gulou District, Fuzhou, Fujian Province, 350001, People's Republic of China, Tel +86-591-83357896, Email weiqunguandr_12@163.com

Objective: Oral lichen planus (OLP) is a chronic inflammatory disorder with malignant potential. The aim is to characterize serum exosome protein expression profiles in patients diagnosed with OLP and to identify potential disease-associated candidate proteins.

Methods: Serum samples were collected from 30 participants, comprising erosive OLP patients, non-erosive OLP patients, and healthy controls (n = 10 per group). Serum exosome proteomes were compared across groups following validation of exosomal integrity using nanoparticle tracking analysis (NTA), transmission electron microscopy (TEM), and Western blotting. Label-free quantitative proteomic profiling was performed with Orbitrap Exploris 480 mass spectrometry, integrated with bioinformatics analyses to identify differentially expressed proteins.

Results: About 138 differentially expressed proteins (DEPs, 39↑/99↓) in OLP patients vs controls, with subtype-specific profiles (70 DEPs in non-erosive, 99 in erosive). Gene Ontology (GO) enrichment analysis indicated that these proteins were predominantly associated with extracellular vesicles, protein binding, and immune response regulation. Kyoto Encyclopedia of Genes and Genomes (KEGG) pathway analysis highlighted enrichment in the complement and coagulation cascade ($p < 0.05$), platelet activation, and focal adhesion pathways. Protein-protein interaction (PPI) network analysis identified central proteins including fibronectin 1 (FN1), complement component 3 (C3), integrin subunit beta 3 (ITGB3), vinculin (VCL), and SRC proto-oncogene (SRC). Among these, FN1 and C3 were implicated in mediating epithelial-extracellular matrix (ECM) separation and thromboinflammatory activity.

Conclusion: The identified differentially expressed proteins in serum exosomes and their association with the complement and coagulation cascade pathway appear to contribute to the pathogenesis and progression of OLP. FN1 and C3 dysregulation directly contributes to OLP pathogenesis via immune-stromal crosstalk. Core proteins such as FN1 and C3 may serve as promising non-invasive diagnostic biomarkers and therapeutic targets, warranting further validation.

Keywords: oral lichen planus, proteomics, serum exosome, bioinformatics, complement-coagulation cascade

Introduction

Oral lichen planus (OLP) is a chronic inflammatory condition of the oral mucosa with a pathogenesis that remains incompletely understood. It commonly presents with mucosal irritation, xerostomia, pain, and other inflammatory symptoms, resulting in diminished quality of life for affected patients. Clinically, OLP is classified into two major forms: the non-erosive type, which is characterized by white striae, and the erosive type, which is associated with mucosal ulceration and greater discomfort.[1] The condition affects approximately 0.5% to 2% of the general population.[2] Notably, OLP carries a risk of malignant transformation, with reported carcinogenesis rates ranging from 0.44% to 2.28%.[3] In addition, there is an increased risk of malignant transformation in patients with erosive and/or atrophic lesions, tongue lesions, high alcohol or tobacco consumption, and coexisting hepatitis C virus infection.[4]

Received: 14 July 2025
Accepted: 11 September 2025
Published: 26 September 2025

The etiology of OLP is not yet fully understood, with potential contributing factors, including immune dysregulation, microbial infection, local mucosal trauma or chronic irritation, and genetic predisposition.[5–7] Among these, immune dysregulation is currently regarded as a principal component in disease development.[8] Specifically, aberrant T-cell-mediated immune responses may target the oral mucosa and initiate apoptosis of basal epithelial cells.[9] Further investigation into the mechanisms of OLP pathogenesis is essential to improve diagnostic accuracy, optimize therapeutic strategies, and ultimately reduce patient burden.

Exosomes are small, cell-derived extracellular vesicles measuring approximately 50 to 200 nm in diameter. These vesicles encapsulate molecular contents reflective of their cells of origin and serve as key mediators of intercellular communication. Exosomes are involved in various physiological and pathological processes, including immune modulation, regulation of cellular differentiation, and facilitation of viral transmission.[10–12] Owing to their diverse biological functions, exosomes have emerged as promising candidates for disease diagnostics, therapeutic development, and biomarker discovery.[13]

Previous studies on exosomes in OLP have primarily focused on the RNA level. Plasma exosomes from OLP patients showed significantly upregulated miR-34a-5p, Hcmv-miR-UL59 from OLP patients.[14,15] Analysis of salivary exosomes from OLP patients found that miR-4484, miR-1246, and miR-1290 are enriched miRNAs in OLP, with miR-4484 being significantly upregulated by Byun et al's analysis.[16]

Due to inconsistencies between gene and protein levels, and given that protein diversity far exceeds that of genes and involves more complex classification, further research into the protein components of serum exosomes in OLP is warranted.

Experimental Section

In this study, serum samples were collected from healthy individuals and patients diagnosed with different OLP subtypes (erosive, non-erosive). Through comparative proteomic profiling of serum exosomes, we aimed to identify disease-associated proteins that could serve as novel therapeutic targets and prognostic biomarkers at the serum protein level.

Research Participants

Patients diagnosed with OLP who visited the Department of Oral Mucosa at Fujian Medical University Union Hospital between September 1, 2023, and December 31, 2023, and who met the inclusion criteria, were enrolled in this study. The required sample size was determined using PASS 15.0.5 software with a test power of 0.90 and an allowable error of 1%, resulting in a target of 20 patients. Given the higher prevalence of OLP among women, the enrolled cohort consisted of 4 male and 16 female patients, with ages ranging from 27 to 68 years (mean age: 53 ± 9 years).[17] The control group comprised 10 healthy individuals from the medical staff at Fujian Medical University Union Hospital. These individuals had no documented medical history and exhibited no clinical signs of OLP upon examination. The control group included 2 males and 8 females, aged 32 to 58 years (mean age: 50 ± 7 years). Informed consent was obtained from all participants prior to inclusion, and ethical approval was granted by the Ethics Committee of Fujian Medical University Union Hospital (approval no. 2023KY064).

Inclusion criteria: (1) Clinical features consistent with non-erosive OLP (slightly elevated white lacy striae forming reticular or radial lesions or white plaques on the oral mucosa) or erosive OLP (presence of mucosal erosion and ulcers), with diagnosis confirmed by tissue biopsy and histopathology, according to the World Health Organization definition of OLP. (2) Absence of systemic diseases, including infectious, allergic, or autoimmune conditions. (3) Absence of other known oral mucosal disorders. (4) No evidence of gingivitis or periodontitis.

Histopathological criteria: Presence of a well-defined, band-like lymphocytic infiltration confined to the superficial connective tissue, accompanied by liquefaction degeneration of the basal cell layer, and absence of epithelial dysplasia.

Exclusion criteria: (1) History of smoking or alcohol abuse; current pregnancy or lactation. (2) Concurrent infectious, allergic, cardiovascular, hematological, or endocrine disorders. (3) Use of systemic or topical anti-inflammatory or immunomodulatory drugs within the past 3 months. (4) Presence of oral lichenoid reactions, including lichenoid contact reactions and drug-induced lichenoid eruptions.

Main Experimental Instruments and Reagents

Four degrees Celsius centrifuge Fresco 17 (Thermo Fisher Scientific Inc., USA), room temperature centrifuge Pico21 (Thermo Fisher Scientific Inc., USA), automated chemiluminescence image analysis system Tanon 5200 (Shanghai Tanon Science & Technology Co., Ltd., China), nanoparticle tracking analyzer ZetaVIEW S/N 17–310 (Particle Metrix Company, Germany), nano transmission electron microscope Tecnai G2 Spirit BioTwin (FEI Company, USA), mass spectrometer Orbitrap Exploris 480 + FAIMS (Thermo Fisher Scientific Inc., USA), high performance liquid chromatography (HPLC) liquid chromatography system EASY-nLC 1200 (Thermo Fisher Scientific Inc., USA), MonoSpin C18 desalting column (GL Sciences Inc., Japan), mass spectrometry data analysis software: Proteome Discoverer 2.4 (Sequent HT) (Thermo Fisher Scientific Inc., USA).

qEV size exclusion chromatography (SEC) column for exosome isolation qEVoriginal (IZON Company, New Zealand), anti-tumor susceptibility gene 101 (TSG101), ALIX, calnexin antibody (System Biosciences, USA), Goat anti-Rabbit HRP (180202–001, System Biosciences, USA), Goat anti-Rabbit HRP (180202–002, System Biosciences, USA), urea (51456–500G, Sigma-Aldrich Corporation, USA), sodium dodecyl sulfate (SDS) (A500228-0001, Sangon Biotech (Shanghai) Co., Ltd., China), Bicinchoninic Acid (BCA) quantification kit P0009 (Beyotime Biotechnology Co., Ltd., China), BeriBLOT detection reagent ab131366 (Abcam Company, UK), Anti-mouse IgG (HRP) ab131368 (Abcam Company, UK).

Sample Collection and Processing

Samples were collected from each participant individually. All participants were instructed to fast and refrain from drinking liquids after 8:00 PM the night prior to sample collection.[18] At 8:00 AM, venous blood was drawn. Following centrifugation, 1 mL of serum was isolated and stored at −80°C until further analysis.

Serum Exosome Extraction

Exosome isolation and purification were performed as follows. Serum samples were thawed in a 25°C water bath and then incubated on ice. Sequential gradient centrifugation was conducted at 4°C: first at 2,000 × g for 10 minutes, followed by 10,000 × g for 30 minutes. The resulting supernatant was collected at each step. Column chromatography purification was then performed. A 500 μL aliquot of the sample was loaded onto the column after discarding the initial buffer. The bottom cap of the SEC column was removed to collect successive 0.5 mL fractions. The first 3 mL (void volume) was discarded. Once the sample reached the top screen of the column, additional buffer was added, and a 1.5 mL high-purity exosome fraction was collected. For ultrafiltration concentration, the ultrafiltration tube was pre-activated by pre-cooling in an ice bath, followed by filtration with ultrapure water for 5 minutes. A sample volume ≤ 4 mL was then loaded and centrifuged at 7,500 × g for 30 minutes. The final product was resuspended in 1× phosphate-buffered saline (PBS) by vortexing and recovered by washing the membrane surface five times to ensure complete yield.

Serum Exosome Characterization and Validation

Exosome Protein Extraction and Quantification

A defined volume of exosome PBS resuspension was collected, and an equal volume of radio-immunoprecipitation assay (RIPA) buffer was added for lysis and protein extraction. The mixture was incubated at 4°C for 30 minutes, with agitation every 10 minutes. Following lysis, samples were centrifuged at 13,200 rpm for 15 minutes at 4°C. The resulting supernatant was transferred to a new centrifuge tube. Protein concentration of the exosomes was determined using a BCA assay working solution.

Exosome WB Identification

Gel electrophoresis was conducted based on the molecular weight of the target protein using 1.5 mm thick glass plates and 15-well sample combs. Initial electrophoresis was performed at a constant voltage of 80 V until the loading buffer indicator reached the separating gel, after which the voltage was increased to 120 V and continued until the indicator reached the bottom of the gel. Membrane transfer was carried out using a polyvinylidene fluoride (PVDF) membrane with a pore size of 0.22 μm under a constant current of 200 mA for 90 minutes. The membrane was then blocked with 5% skim milk powder diluted in PBS with Tween® 20 (PBST) for 1 hour. After 30 minutes of PBST washing, the membrane was incubated

overnight at 4°C with the primary antibody in a hybridization box. The following day, after returning to room temperature and additional PBST washing for 30 minutes, the membrane was incubated with the corresponding secondary antibody for 1 hour at room temperature under gentle agitation. After further washes, enhanced chemiluminescence (ECL) substrate was added dropwise, and signal detection was performed using a digital imaging system with continuous exposure.

Nanoparticle Tracking Analysis

Stored frozen samples were thawed in a 25°C water bath and subsequently placed on ice. Exosome samples were diluted using 1× PBS and directly analyzed using nanoparticle tracking analysis (NTA).

Transmission Electron Microscopy Detection

A 5 μL aliquot of the exosome sample was deposited onto a copper grid and incubated at room temperature for 5 minutes. Excess liquid was gently removed using absorbent paper. One drop of 2% uranyl acetate was added to the grid and incubated for 1 minute at room temperature. Excess solution was removed using absorbent paper, and the grid was air-dried for 20 minutes before observation under the transmission electron microscope (TEM).

Label-Free Quantitative Proteomics Analysis

Proteomic sample preparation was conducted as follows: 10 μL of magnetic beads were washed with PBS and resuspended in 25 μL PBS. The exosome samples were added, and two incubation cycles of 5 minutes each were performed to allow binding. Following magnetic separation and removal of the supernatant, 100 μL lysis buffer (containing 7 M urea, 2% SDS, and 1× protease inhibitor) was added. After vortex mixing, the samples underwent ice bath lysis for 30 minutes, followed by centrifugation at 13,000 × g for 20 minutes. The supernatant was collected for protein extraction, and protein concentration was determined using a BCA assay. Subsequently, 20 μg of protein underwent reduction and alkylation (final concentration of 10 mM dithiothreitol [DTT] at 37°C for 1 hour, followed by iodoacetamide [IAA] reaction in the dark for 40 minutes). Proteins were precipitated with five volumes of acetone and centrifuged at 13,000 × g for 1 hour. The resulting pellet was washed twice with acetone, air-dried at room temperature, and subjected to overnight enzymatic digestion with trypsin at 37°C. Peptides were purified using MonoSpin C18 desalting columns through sequential steps: activation with acetonitrile, equilibration with trifluoroacetic acid (TFA), sample loading, washing with TFA, and elution with 50% acetonitrile. The eluted peptides were then concentrated by freeze-drying and stored for subsequent mass spectrometry analysis.

Prior to mass spectrometry, 1 to 2 μg of each sample was reconstituted in 0.1% formic acid. Peptides were separated via a C18 analytical column (1.9 μm, 75 μm × 20 cm) at a flow rate of 200 μL/min. Data-dependent acquisition (DDA) was performed using the Orbitrap Exploris 480 + FAIMS Pro system, with full scan resolution of 60,000 across the m/z range of 350 to 1600. Higher-energy collisional dissociation (HCD) was applied with a fragmentation collision energy of 30%. Mass spectrometry data were searched against a reference database using Proteome Discoverer 2.4 software. Specific search parameters are presented in Table 1.

Table 1 Search Parameters of Proteomics Database

Item	Parameters
Database	Swissprot
Taxonomy	Homo sapiens
Enzyme	Trypsin
Fixed modifications	Carbamidomethyl (C)
Variable modifications	Oxidation (M), Acetyl (Protein N-term)
Max Missed Cleavages	2
Target FDR(Strict)	0.01
Target FDR(Relaxed)	0.05
Min. peptide Length	6
Mass Tolerance	10 ppm

Bioinformatics Analysis

First, Gene Ontology (GO) enrichment analysis was conducted on differentially expressed proteins between groups, using $p < 0.05$ as the significance threshold. The top 10 GO terms with the smallest p values were selected for visualization. Subsequently, Kyoto Encyclopedia of Genes and Genomes (KEGG) pathway enrichment analysis was performed using Fisher's exact test, applying a significance threshold of $p < 0.05$ to identify biological pathways influenced by the experimental conditions. Based on the STRING database (http://string-db.org/), a protein-protein interaction (PPI) network was constructed, applying a high-confidence interaction threshold (>0.9) to ensure the reliability of predicted interactions. Cytoscape 3.10.0 software was used to visualize the network, and topological parameters were calculated using the CytoNCA module. Core hub proteins within the network were identified by assessing betweenness centrality (BC), which served to determine key functional targets for subsequent experimental validation.

Results

Patient General Information

A total of 30 samples were included in the analysis. Age comparisons among the three groups using the Kruskal–Wallis *H*-test indicated no statistically significant difference ($p = 0.096$, > 0.05). Gender distribution across groups was consistent (2 males per 10 patients), and no significant differences in age or gender were observed.

Serum Exosome Characterization

Western blotting (WB) validation demonstrated the presence of exosome marker proteins TSG101 and ALIX in all three groups (non-erosive, erosive, and normal), while the negative control protein Calnexin was undetected (Figure 1A). NTA revealed serum exosome particle concentrations of 6.1×10^{11} particles/mL for the non-erosive group, 2.8×10^{11} particles/mL for the erosive group, and 5.0×10^{11} particles/mL for the normal group. Corresponding peak particle sizes were 108.3 nm (range: 68.1–176.0 nm), 98.6 nm (range: 65.7–166.0 nm), and 104.3 nm (range: 68.5–176.0 nm), respectively (Figure 1B). Transmission electron microscopy (TEM) confirmed the presence of spherical double-membrane vesicle structures characteristic of exosomes in all groups (Figure 1C).

Protein Identification and Differential Protein Screening

Label-free relative quantification was performed using peptide peak intensity (Precursor Intensity) derived from first-level mass spectrometry as the quantitative parameter. Protein expression abundance (Abundance) was calculated through weighted algorithms based on peak intensity. Standardization of peak intensity for each protein across samples yielded the Abundance Normalized values for quantitative analysis. During pairwise group comparisons, mean signal intensity per group was calculated to determine the fold change ratio. Student's *t*-test was applied to calculate inter-group *p* values. Proteins were considered differentially expressed if they met both of the following criteria: (1) fold change ≥ 1.2 or ≤ 0.8333 (ie, 1/1.2); and (2) $p < 0.05$.

Serum Exosome Protein Concentration in Each Group

The measured serum exosome protein concentrations were 0.379 ± 0.177 μg/μL for the non-erosive group, 0.354 ± 0.095 μg/μL for the erosive group, and 0.533 ± 0.273 μg/μL for the normal group. One-way ANOVA analysis revealed no statistically significant difference among the three groups ($p = 0.104$, > 0.05).

Unique Peptide Number Distribution and Peptide Sequence Length Distribution

Figure 2A displays a dual-coordinate distribution chart of the number of unique peptides identified per protein in this study. The horizontal axis represents the number of unique peptides per protein, and the left vertical axis indicates the corresponding protein count. A total of 919 proteins contained two or more unique peptides, accounting for 63.73% of all identified proteins. Figure 2B presents the distribution of peptide lengths identified. The horizontal axis represents peptide length (ie, amino acid count), and the vertical axis indicates the number of peptides of each length. The mean peptide length was 13.61 amino acids, which falls within the expected range for mass spectrometry-derived peptides.

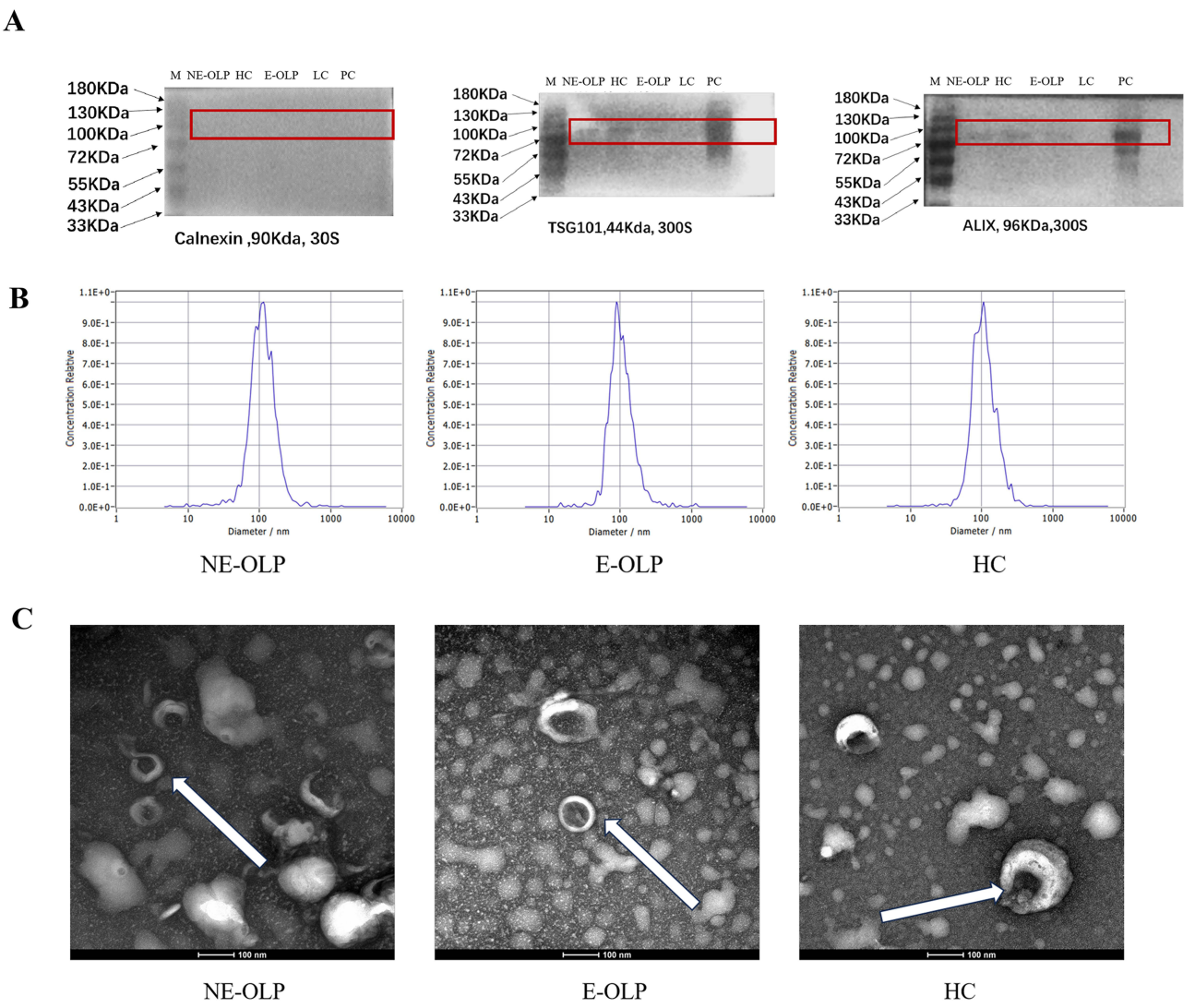

Figure 1 Characterization of serum exosomes. (**A**) Validation of serum exosome surface markers in patients with OLP in the erosion group, non-erosion group, and normal group. Red rectangles highlight electrophoretic bands corresponding to target proteins: TSG101 (45 kDa), ALIX (95 kDa), with absent Calnexin (90 kDa) confirming exosome purity. Molecular weight markers (kDa) shown on left. (**B**) NTA particle size distribution of serum exosomes from non-erosive group, erosive group, and healthy controls, the X-axis represents particle size, and the Y-axis represents relative concentration values. (**C**) TEM characterization of serum exosomes in the erosion group, non-erosion group, and normal group. White arrows indicate characteristic double-membrane vesicles (50–200 nm diameter) in non-erosive OLP, erosive OLP, and healthy controls.

Mass Spectrometry Raw Data Database Search Results

The SwissProt database was utilized for protein identification. A total of 10,849 peptides and 1442 proteins were identified, with 327 proteins meeting the criteria for differential expression. An overview of the differential protein distribution is presented in Table 2. The volcano plot and heatmap comparing the disease group to the normal group are presented in Figure 2C. The volcano plot and heatmap for the non-erosive versus normal group are presented in Figure 2D, and for the erosive versus normal group in Figure 2E. The differential protein expression volcano plot and heatmap for the non-erosive versus erosive group are presented in Figure 2F.

The results showed a total of 138 differentially expressed proteins between the disease group and the normal group. Among these, 39 proteins were upregulated, including those involved in signal transduction and receptor activity such as platelet-derived growth factor subunit B (PDGFB), calcitonin receptor-like receptor (CALCRL), and Ras homolog family member B (RHOB); immune response-associated proteins including human leukocyte antigen-DRB1 (HLA-DRB1), CD46, and complement C3; ECM composition and adhesion molecules such as FN1, LTBP1, and fibulin 1 (FBLN1); as well as proteins involved in metabolism and transport including biotinidase (BTD), dopamine beta-hydroxylase (DBH),

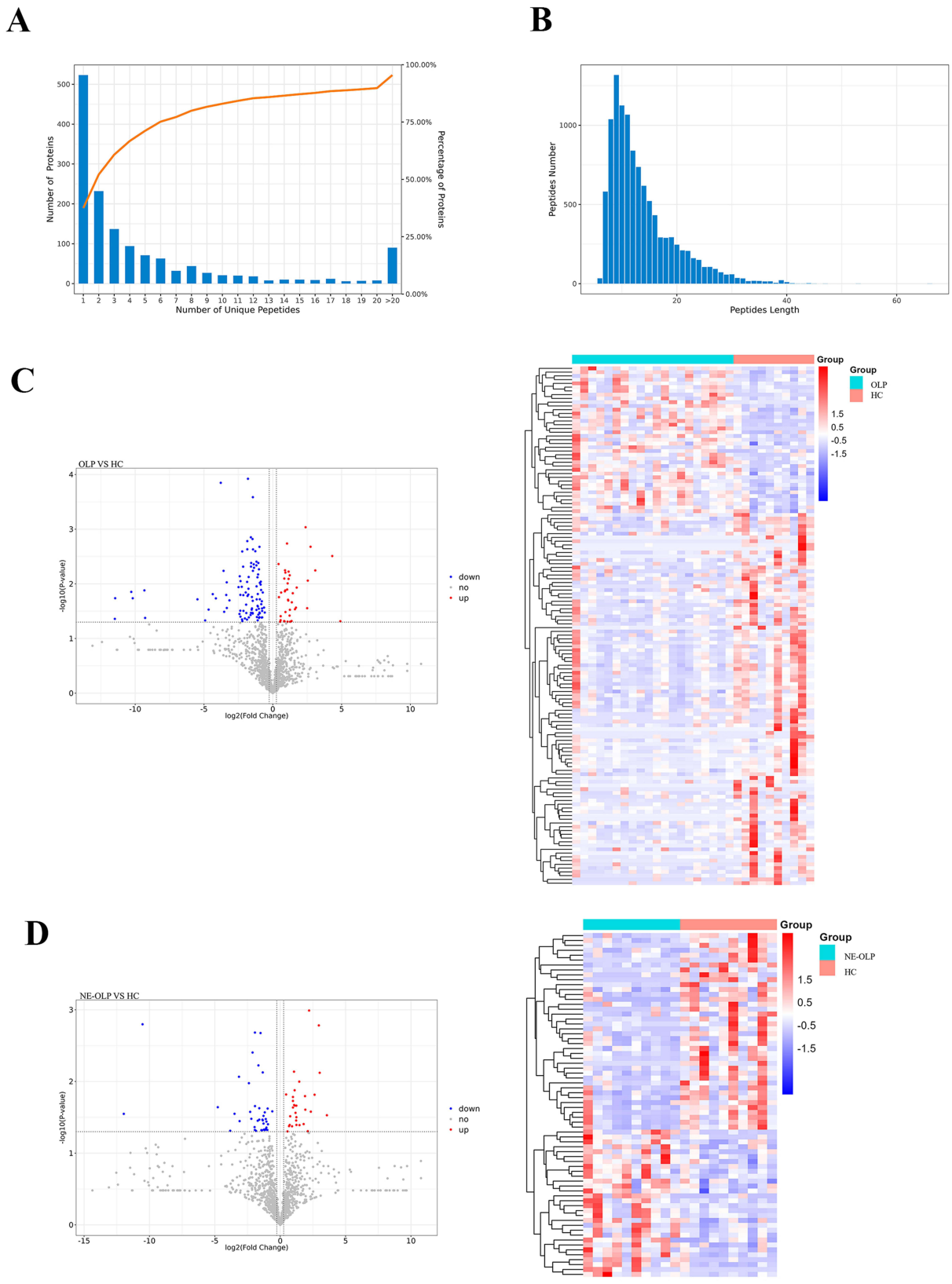

Figure 2 Contiune.

https://doi.org/10.2147/JIR.S553682

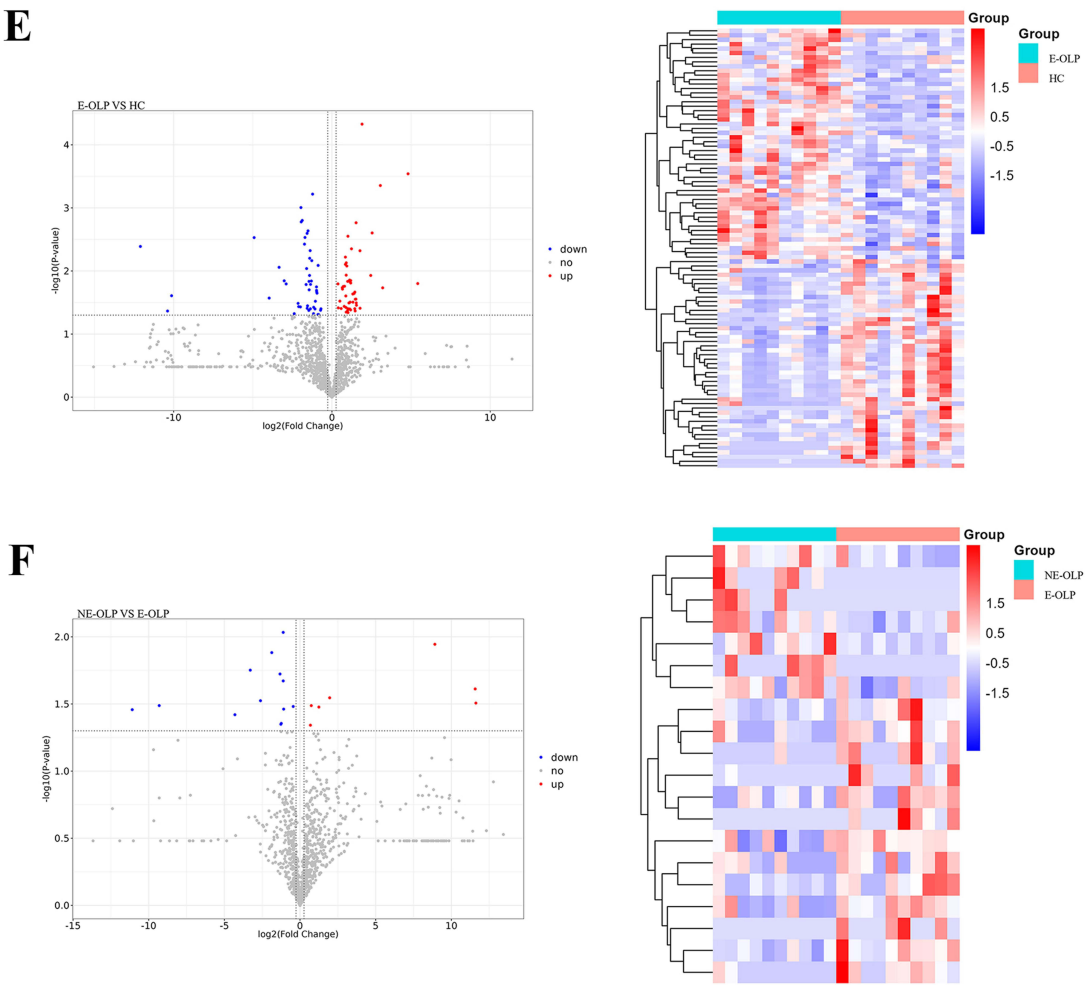

Figure 2 Screening of differentially expressed proteins in serum exosomes between erosive OLP, non-erosive OLP, and normal groups. (**A**) Unique peptide segment distribution chart. The x-axis shows the number of unique peptides per protein. Bars (left y-axis) show the number of proteins with a given peptide count. The curve (right y-axis) shows the cumulative percentage of proteins. (**B**) Distribution of peptide sequence length, with the horizontal axis representing peptide segment length (ie, the number of amino acids contained in the peptide segment) and the vertical axis representing the total number of peptide segments of corresponding lengths. (**C**) Volcanic and heat maps of differential proteins in serum exosomes between the disease group and the normal group. The volcano plot (left) displays statistical significance (-log10(p-value)) versus magnitude of change (log2(fold change)), with red dots indicating upregulated, blue downregulated, and gray non-significant proteins. The heatmap (right) shows a hierarchical clustering of DEPs and samples. Rows represent proteins, columns represent samples, red denotes high expression, and blue denotes low expression. Proteins cluster based on expression similarity, suggesting functional relationships. (**D**) Volcanic and heat maps of differential proteins in serum exosomes between the non-erosion group and the normal group. (**E**) Volcanic and heat maps of differential proteins in serum exosomes between the erosion group and the normal group. (**F**) Volcanic and heat maps of differential proteins in serum exosomes between the non-erosion group and the erosion group.

and low-density lipoprotein receptor (LDLR). Ninety-nine proteins were downregulated, including those related to cytoskeletal structure and adhesion (eg, TLN1, VCL, ITGA2B); signal transduction (eg, RAP1B, type 2 phosphatidylinositol 4,5-bisphosphate 4-phosphatase [PIP4P2], SRC); immune response (eg, human leukocyte antigen-A [HLA-A], ficolin 1 [FCN1], proteasome 20S subunit beta 7 [PSMB7]); and vesicle/membrane transport (eg, syntaxin 11 [STX11], vesicle-associated membrane protein 5 [VAMP5], CD9/CD63).

Table 2 Statistical Table of Differential Proteins Among Groups

Comparison Group	Upregulation of Proteins	Downregulate Proteins	Total Differential Proteins
Disease group/normal group	39	99	138
Non-erosion group/normal group	30	40	70
Erosion group/normal group	52	47	99
Non-erosion group/erosion group	7	13	20

Comparison between the non-erosive group and the normal group identified 70 differentially expressed proteins, of which 30 were upregulated. These included proteins associated with immune responses (eg, HLA-DRB1, immunoglobulin heavy variable 2–70 [IGHV2-70], IGHV3-43, and CD46), coagulation and hematological regulation (eg, carboxypeptidase B2 [CPB2], coagulation factor XIII B chain [F13B], and serpin family F member 2 [SERPINF2]), ECM composition and adhesion (eg, FN1, thrombospondin 4 [THBS4], and FBLN1), as well as signal transduction and receptor-related proteins (eg, CALCRL, RHOB, and transmembrane 4 L six family member 1 [M4SF1]). Forty proteins were downregulated, including those associated with cytoskeletal organization and adhesion (eg, alpha-actinin 1 [ACTN1], VCL, capping actin protein of muscle Z-line subunit alpha 2 [CAPZA2], and tropomyosin 3 [TPM3]); signal transduction (eg, RAP1B, GNA13, RHOG, and FYN); immunity and inflammation (eg, HLA-A, FCN1, and triggering receptor expressed on myeloid cells-like [TREML]); and vesicle/membrane transport (eg, STX11, VAMP5, and tetraspanin 33 [TSPAN33]).

In the comparison between the erosive group and the normal group, 99 differentially expressed proteins were identified, including 52 upregulated proteins. These included those associated with signal transduction (eg, PDGFB, CALCRL, RHOB), immune response (eg, HLA-DRB1, CD46, C3), coagulation and fibrinolysis (eg, SERPINA10, kallikrein B1 [KLKB1], fibrinogen alpha chain [FGA]), ECM and adhesion (eg, FN1, extracellular matrix protein 1 [ECM1], collagen type VI alpha 1 chain [COL6A1]), and metabolism/transport (eg, BTD, DBH, LDLR). Forty-seven proteins were downregulated, including those involved in adhesion and cytoskeletal organization (eg, calponin-2 [CNN2], ITGA2B, ITGB3, VCL); signal transduction and metabolism (eg, PIP4P2, YWHAB, YWHAQ, PLA2G7); immune regulation (eg, ITGAM, C-X-C motif chemokine receptor 2 [CXCR2], ADP-ribosyltransferase 4 [ART4]); and vesicle/membrane transport (eg, DCTN2, solute carrier family 44 member 1 [SLC44A1], and CD9).

Comparison between the non-erosive and erosive groups revealed 20 differentially expressed proteins, including 7 upregulated proteins. These were involved in metabolic regulation (eg, solute carrier family 25 member 6 [SLC25A6], lipoprotein lipase [LPL]), cytoskeletal and adhesion components (eg, TPM3, desmoglein 1 [DSG1]), immune and inflammatory response (eg, interleukin-1 receptor accessory protein [IL1RAP]), and ECM or signaling pathways (eg, THBS4, coiled-coil domain-containing protein 13 [CCDC13]). Thirteen proteins were downregulated, including immune-related proteins (eg, IGHV1-2, pulmonary surfactant-associated protein A1 [SFTPA1], and TREML1) and those involved in adhesion and signal regulation (eg, neural cell adhesion molecule 1 [NCAM1], integrin subunit alpha 4 [ITGA4], and CALCRL/tescalcin [TESC]).

Basic Bioinformatics Analysis of Serum Exosome Differential Proteins Between OLP Disease Group and Normal Group

GO Enrichment Analysis of Serum Exosome Differential Proteins Between OLP Disease Group and Normal Group

GO enrichment analysis was conducted on differential proteins identified between the disease group and the normal group. Within the Biological Process (BP) category, proteins were primarily associated with cell adhesion, regulation of cell adhesion, response to wound, and wound healing. In the Cellular Component (CC) category, enrichment was mainly observed in vesicles, extracellular region, and extracellular space. Molecular Function (MF) analysis indicated enrichment in homoprotein binding, protein complex binding, and signal receptor binding, as presented in Figure 3A.

KEGG Pathway Enrichment Analysis of Serum Exosome Differential Proteins Between OLP Disease Group and Normal Group

KEGG pathway enrichment analysis was applied to the differentially expressed proteins between the disease and normal groups. The 15 pathways with the lowest *p* values included SNARE interactions in vesicular transport, bacterial invasion of epithelial cells, platelet activation, hematopoietic cell lineage, complement and coagulation cascades, focal adhesion, extracellular matrix (ECM)-receptor interaction, hypertrophic cardiomyopathy, dilated cardiomyopathy, regulation of actin cytoskeleton, cytoskeletal dynamics in muscle cells, phagosome, proteoglycans in cancer, and the Rap1 signaling pathway, as presented in Figure 3B.

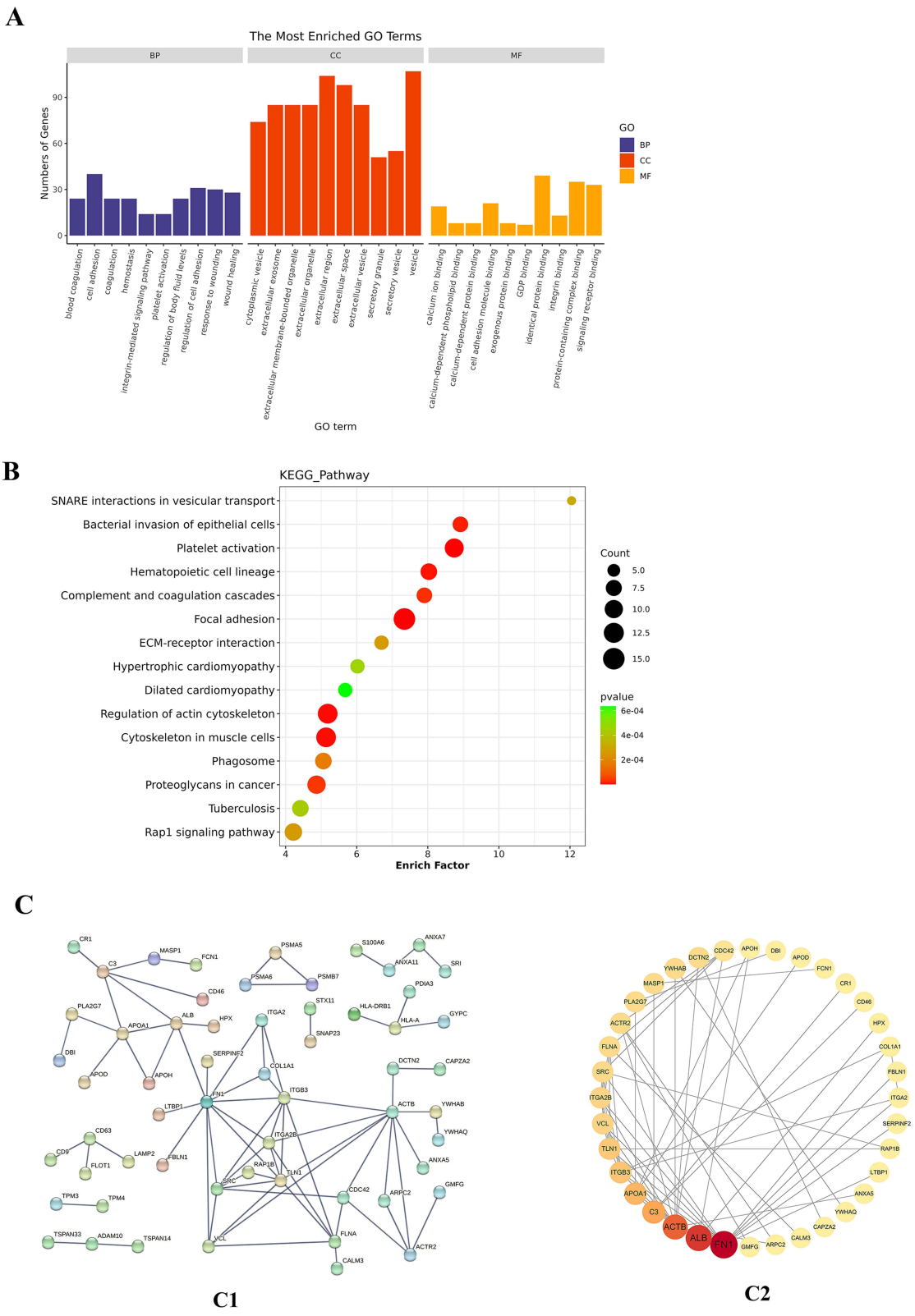

Figure 3 Biological information analysis of proteins differing between normal group and OLP disease group based on serum exosome samples. (**A**) Enrichment analysis of differential protein GO in serum exosomes between the disease group and the normal group. Plot the 10 entries with the smallest p-values. The vertical axis represents the number of counts (the number of genes matched to that entry), and the horizontal axis represents the entry. (**B**) Enrichment analysis of differential protein KEGG pathways in serum exosomes between the disease group and the normal group. The top 15 most significant terms (smallest p-values) are displayed. The x-axis shows the enrichment factor; the y-axis lists the pathway terms. Point color corresponds to the p-value (significance level), and point size represents the number of matched proteins (Count). (**C**) Analysis of the interaction of differential protein networks of serum exosomes between the disease group and the normal group. Fig. 3C2 shows the top 20 proteins with the highest BC values. The darker the color and the larger the dot, the higher the BC value. Solid edges represent high-confidence interactions (STRING score > 0.9).

Network Interaction Analysis of Serum Exosome Differential Proteins Between OLP Disease Group and Normal Group

Protein-protein interaction (PPI) analysis was conducted on differential proteins between the disease and normal groups. The top 20 proteins ranked by BC included: fibronectin 1 (FN1), albumin (ALB), actin beta (ACTB), complement C3 (C3), apolipoprotein A-I (APOA1), integrin subunit beta 3 (ITGB3), talin 1 (TLN1), integrin subunit alpha 2b (ITGA2B), vinculin (VCL), SRC proto-oncogene (SRC), filamin A (FLNA), actin-related protein 2/3 complex subunit 2 (ACTR2), mannan-binding lectin serine peptidase 1 (MASP1), phospholipase A2 group VII (PLA2G7), dynactin subunit 2 (DCTN2), tyrosine 3-monooxygenase/tryptophan 5-monooxygenase activation protein beta (YWHAB), cell division cycle 42 (CDC42), tyrosine 3-monooxygenase/tryptophan 5-monooxygenase activation protein theta (YWHAQ), RAS-related protein 1B (RAP1B), and latent transforming growth factor beta binding protein 1 (LTBP1), as presented in Figure 3C.

Basic Bioinformatics Analysis of Serum Exosome Differential Proteins Between OLP Non-Erosive Group and Normal Group

GO Enrichment Analysis of Serum Exosome Differential Proteins Between OLP Non-Erosive Group and Normal Group

GO enrichment analysis of differentially expressed proteins between the non-erosive group and the normal group demonstrated that biological process terms were primarily enriched in response to stress, immune system processes, and regulation of immune system processes. Cellular component terms were predominantly associated with the extracellular region, vesicles, and extracellular space. Molecular function terms were concentrated in homoprotein binding, protein complex binding, and signal receptor binding, as presented in Figure 4A.

KEGG Pathway Enrichment Analysis of Serum Exosome Differential Proteins Between OLP Non-Erosive Group and Normal Group

KEGG pathway enrichment analysis of differentially expressed serum exosome proteins between the non-erosive and normal groups revealed that the top 15 pathways with the smallest p values included viral myocarditis, complement and coagulation cascades, adherens junction, bacterial invasion of epithelial cells, long-term potentiation, platelet activation, focal adhesion, antigen processing and presentation, leukocyte transendothelial migration, phagosome, cytoskeletal regulation in muscle cells, vascular smooth muscle contraction, oocyte meiosis, regulation of actin cytoskeleton, and viral carcinogenesis, as presented in Figure 4B.

Basic Bioinformatics Analysis of Serum Exosome Differential Proteins Between OLP Erosive Group and Normal Group

GO Enrichment Analysis of Serum Exosome Differential Proteins Between OLP Erosive Group and Normal Group

GO enrichment analysis was conducted on the differential proteins identified between the erosive group and the normal group. Enrichment in the biological process category was primarily observed in the establishment of localization, regulation of response to stimulus, response to stress, and transport. Cellular component terms were mainly enriched in the extracellular region, extracellular space, and vesicles. Molecular function terms were predominantly associated with enzyme binding, homoprotein binding, protein complex binding, and signal receptor binding, as presented in Figure 5A.

KEGG Pathway Enrichment Analysis of Serum Exosome Differential Proteins Between OLP Erosive Group and Normal Group

KEGG pathway enrichment analysis of the differential proteins between the erosive and normal groups revealed that the top 15 pathways with the smallest p values included the renin-angiotensin system, complement and coagulation cascades, hematopoietic cell lineage, leishmaniasis, ECM-receptor interaction, amoebiasis, platelet activation, focal adhesion, leukocyte transendothelial migration, regulation of actin cytoskeleton, phagosome, Rap1 signaling pathway, neutrophil extracellular trap formation, cytoskeletal regulation in muscle cells, and the phosphatidylinositol 3-kinase-protein kinase B (PI3K-AKT) signaling pathway, as presented in Figure 5B.

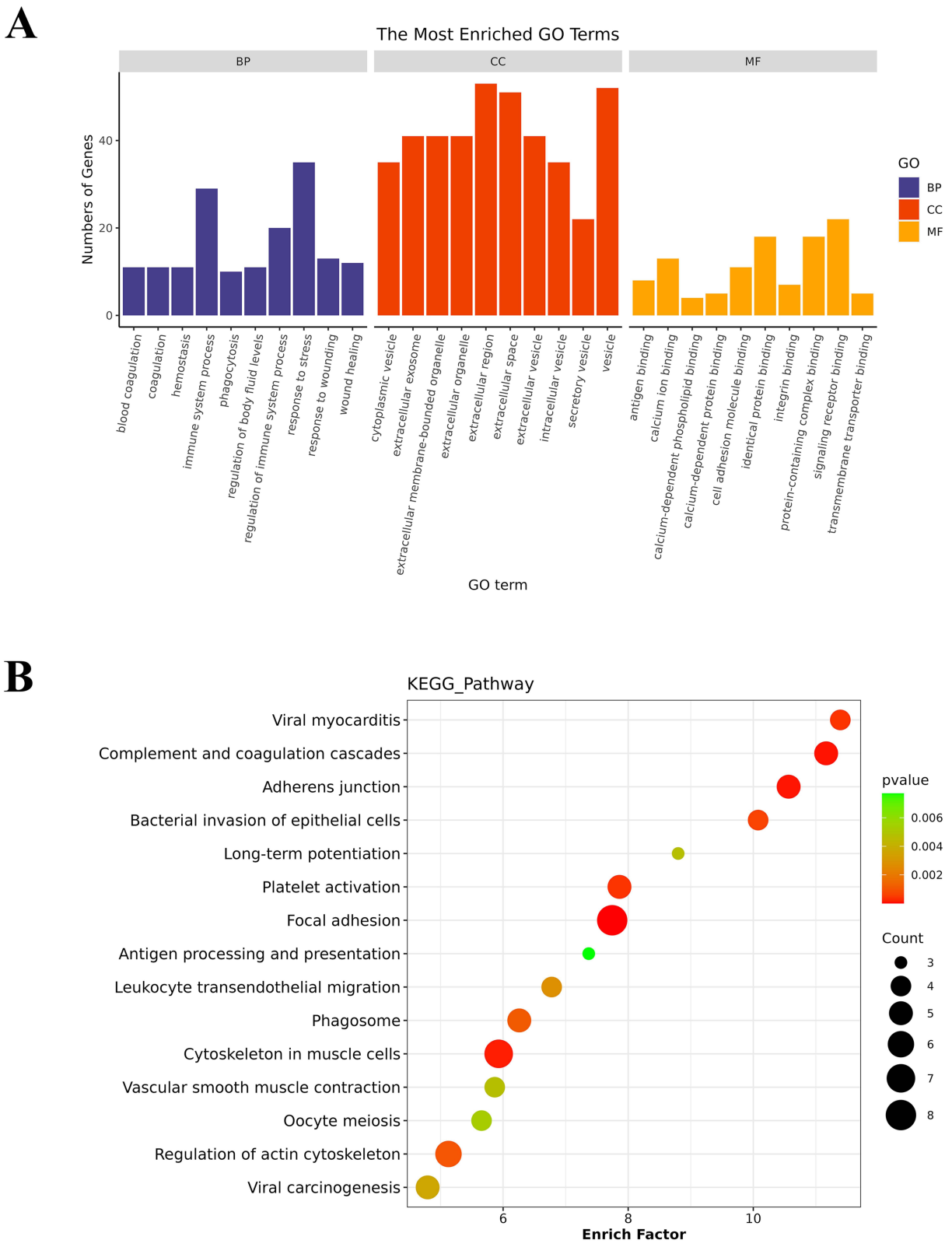

Figure 4 Biological information analysis of proteins differing between non-erosive OLP group and normal group based on serum exosome samples. (**A**) Enrichment analysis of differential protein GO in serum exosomes between the non-erosion group and the normal group. (**B**) Enrichment analysis of differential protein KEGG pathways in serum exosomes between the non-erosion group and the normal group.

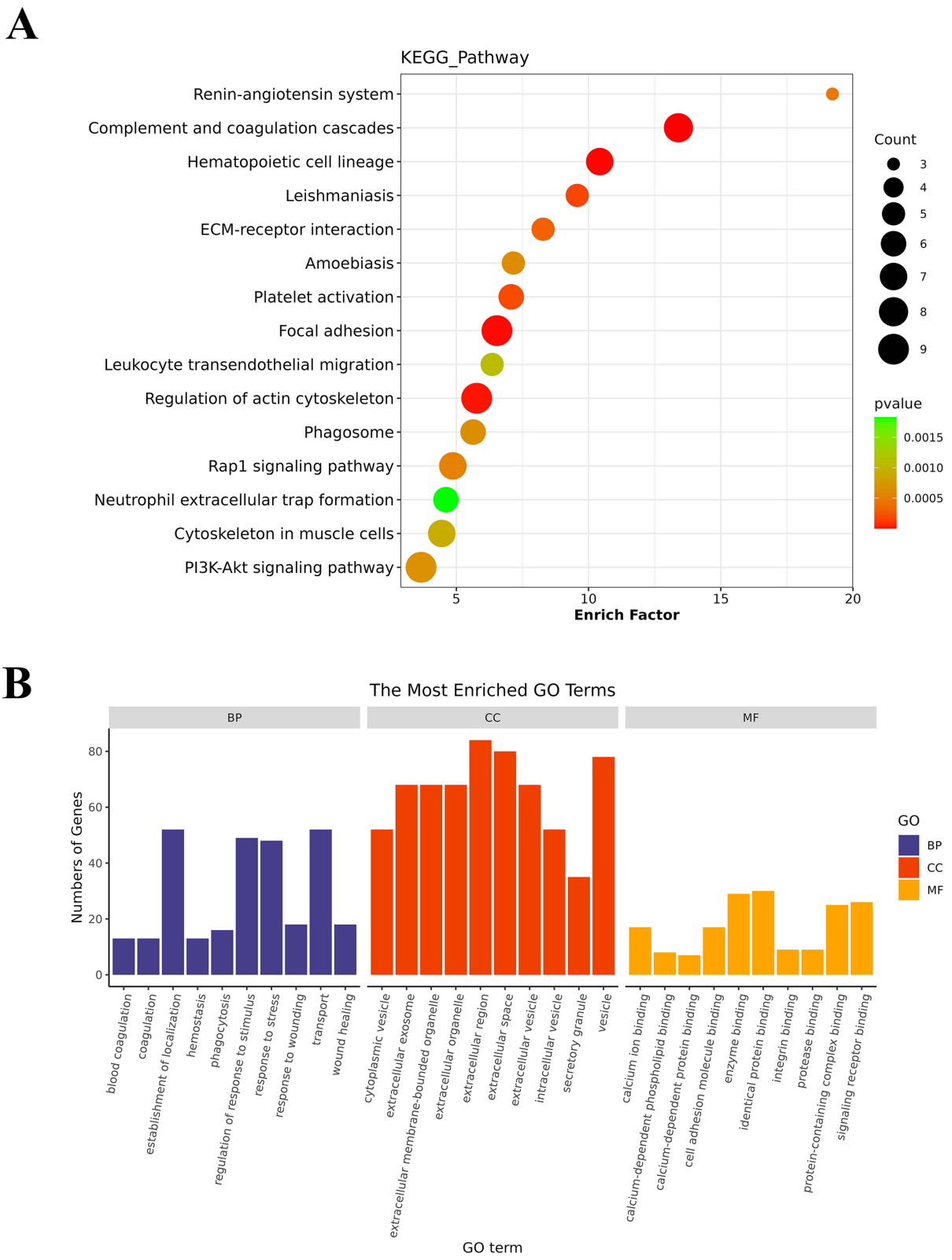

Figure 5 Biological information analysis of proteins differing between erosive OLP group and normal group based on serum exosome samples. (**A**) Enrichment analysis of differential protein GO in serum exosomes between the erosion group and the normal group. (**B**) Enrichment analysis of differential protein KEGG pathways in serum exosomes between the erosion group and the normal group.

https://doi.org/10.2147/JIR.S553682

Basic Bioinformatics Analysis of Serum Exosome Differential Proteins Between OLP Non-Erosive Group and OLP Erosive Group

GO Enrichment Analysis of Serum Exosome Differential Proteins Between OLP Non-Erosive Group and OLP Erosive Group

GO enrichment analysis was conducted on the differential proteins identified between the non-erosive and erosive groups. In the biological process category, proteins were mainly enriched in response to carbohydrate, response to organic substance, and response to oxygen-containing compound. Cellular component terms were primarily concentrated in the extracellular region, extracellular space, and vesicles. Molecular function terms were mostly related to calcium ion binding, protein homodimerization activity, and protein complex binding, as presented in Figure 6A.

KEGG Pathway Enrichment Analysis of Serum Exosome Differential Proteins Between OLP Non-Erosive Group and OLP Erosive Group

KEGG pathway enrichment analysis of differential serum exosome proteins between the non-erosive and erosive groups demonstrated that the top 15 enriched pathways with the lowest *p* values included those related to viral particles—Ebola virus, hemolytic virus, and measles virus, as well as cholesterol metabolism, thyroid cancer, peroxisome proliferator-activated receptor (PPAR) signaling pathway, ECM-receptor interaction, intestinal immune network for IgA production, hypertrophic cardiomyopathy, malaria, dilated cardiomyopathy, cytoskeletal regulation in muscle cells, phagosome, cell adhesion molecules, focal adhesion, prion disease, and human papillomavirus infection, as presented in Figure 6B.

Discussion

Exosomes originate from vesicle interiors. The process begins with the invagination of the cell membrane, leading to the formation of endocytic vesicles. These vesicles subsequently incorporate intracellular proteins, enzymes, and various biomolecules during continuous fusion processes, eventually maturing into multivesicular bodies (MVB). MVBs may either fuse with the cell membrane to release exosomes into the extracellular space or be directed to lysosomes for degradation.[19] The transported substances are involved in numerous physiological and pathological processes.

In this study, vesicle components were extracted using the qEV reagent kit based on SEC, followed by a triple-characterization strategy comprising TEM for morphology, NTA for particle size, and validation of exosome marker proteins. The isolated vesicle population demonstrated typical exosomal morphological characteristics, with surface marker expression consistent with classical exosome profiles and particle sizes within the expected exosomal distribution range.

Quantitative proteomics based on mass spectrometry (MS) represents the current standard for analyzing the overall protein composition of biological samples. Core steps include protein/peptide separation from clinical samples, mass spectrometry detection, and subsequent data processing to elucidate protein structure, abundance, function, and interaction networks.[20] In this study, a label-free quantitative proteomics approach was employed to analyze serum exosome proteins. The measured serum exosome protein concentrations were 0.379 ± 0.177 μg/μL in the non-erosive group, 0.354 ± 0.095 μg/μL in the erosive group, and 0.533 ± 0.273 μg/μL in the normal group. No statistically significant difference in protein concentration was identified among the three groups.

Compared with the normal group, the OLP disease group showed upregulation of proteins involved in signal transduction and receptor activity, such as PDGFB, as well as proteins related to immune response, including HLA-DRB1, CD46, and C3. Among the downregulated proteins, PSMB7 is also related to immune processes. Previous studies have found that PDGFB promotes cellular proliferation, differentiation, and migration during angiogenesis and tissue development and has been implicated in the pathogenesis of vascular, fibrotic, and neoplastic disorders.[21] The established immunopathological mechanism in OLP involves CD8+ cytotoxic T cell-mediated apoptosis of basal keratinocytes and the establishment of a chronic inflammatory microenvironment by CD4+ helper T cells.[22] The elevated expression of HLA-DRB1 in the disease group may facilitate the presentation of self-antigen peptides to CD4+ T cells, potentially resulting in excessive secretion of proinflammatory cytokines such as interferon gamma (IFN-γ) and tumor necrosis factor alpha (TNF-α).[23] Additionally, the downregulation of PSMB7 may impair antigen processing, resulting in abnormal antigen accumulation and immune dysregulation.[24]

There were a total of 70 differentially expressed proteins between the non-erosive group and the normal group, among which the upregulated proteins were enriched in proteins related to immune response, including HLA-DRB1,

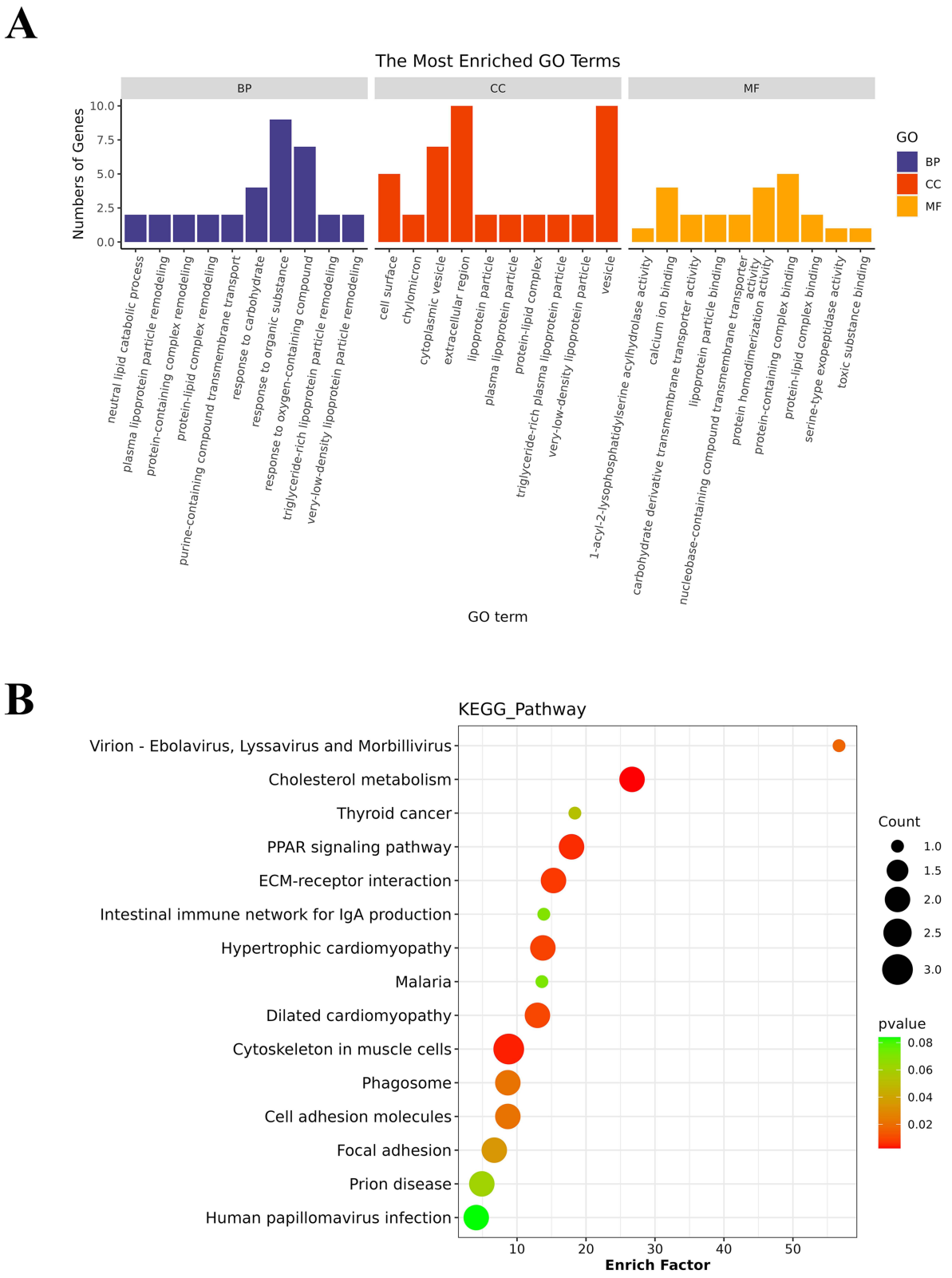

Figure 6 Biological information analysis of proteins differing between non-erosive OLP group and erosive OLP group based on serum exosome samples. (**A**) Enrichment analysis of differential protein GO in serum exosomes between the non-erosion group and the erosion group. (**B**) Enrichment analysis of the KEGG pathway of differential proteins in serum exosomes between the non-erosion group and the erosion group.

https://doi.org/10.2147/JIR.S553682

IGHV2-70, IGHV3-43, CD46; downregulated proteins were associated with cytoskeletal and adhesion proteins (such as ACTN1, VCL, CAPZA2, TPM3), immune and inflammatory proteins (like FCN1), and membrane transport and vesicle-related proteins (including STX11). The upregulation of HLA-DRB1 and immunoglobulin heavy chain genes (IGHV2-70 and IGHV3-43) indicated activation of autoimmune mechanisms.[25] The increased expression of the complement regulatory protein CD46 may indicate an attempt to inhibit complement overactivation, block C3b deposition, and regulate metabolic adaptation during T cell activation.[26] Conversely, the downregulation of FCN1 likely reflected dysfunction in the lectin complement pathway, reducing chemotaxis, phagocytosis, and antigen presentation by immune cells, thereby weakening adaptive immune responses and maintaining a state of chronic inflammation.[27]

Upregulated ECM components such as FN1, THBS4, and FBLN1 are known to promote collagen cross-linking, leading to mucosal stiffening and characteristic whitening and hardening observed in non-erosive OLP.[28] In contrast, the downregulation of cytoskeletal proteins (eg, VCL and ACTN1) and adhesion-related proteins (eg, CAPZA2 and TPM3) was consistent with histopathological manifestations such as reticular lesions. STX11, a soluble NSF attachment protein receptor (SNARE), facilitates cytotoxic granule fusion at the immunological synapse of CD8+ T and natural killer (NK) cells.[29] Reduced STX11 expression may disrupt SNARE complex assembly, impairing exosome secretion and cytotoxic synapse formation, and contributing to the observed CD8+ T cell accumulation in lesional tissues.

Differences between the erosive group and the normal group include upregulation of proteins involved in signal transduction regulation and immune response, such as C3, SERPINA10, and KLKB1, which are related to coagulation and fibrinolysis. Downregulated proteins are involved in cell adhesion and cytoskeletal regulation, signal transduction and metabolic regulation, immune and inflammatory responses, and membrane transport and vesicle formation. Hyperactivation of complement component C3 may result in excessive C3b deposition and formation of C5 convertase, which facilitates membrane attack complex (MAC) formation and leads to direct keratinocyte lysis.[30] Increased KLKB1 expression may trigger activation of coagulation factor XII (FXII), promoting thrombin burst generation and causing local microvascular thrombosis, which is histologically manifested as necrosis and epithelial erosion.[31] Simultaneously, upregulation of SERPINA10 may suppress FXa and plasmin activity, thereby impairing tissue repair and contributing to delayed healing of erosive lesions.[32]

The main upregulated proteins between the non-erosive group and the erosive group were SLC25A6 and LPL, which are involved in metabolic regulation; DSG1, which is related to the cytoskeleton and adhesion; and THBS4, which is involved in the construction of the extracellular matrix (ECM) and signaling. The downregulated proteins were related to immunity, cell adhesion, and signaling. These differential expression patterns indicate that the transition from non-erosive to erosive OLP may reflect a shift toward "reparative inflammation and metabolic adaptation." The upregulation of THBS4, a pro-fibrotic ECM protein, may accelerate basement membrane stiffening, while DSG1 elevation enhances intercellular adhesion, potentially limiting lateral spread of epithelial lesions.[33] Concurrently, upregulation of SLC25A6 may improve mitochondrial ATP production, and elevated LPL may support lipid metabolism via triglyceride hydrolysis and free fatty acid release. These changes may collectively support high-energy tissue repair processes in areas of epithelial erosion, indicating that erosive OLP represents a state of compensatory reparative inflammation.

In the serum exosome proteomics analysis of OLP, the disease state demonstrated notable differences compared to the normal group. Upregulated proteins, including signal transduction factors (PDGFB, CALCRL), immune molecules (HLA-DRB1, C3), and ECM components (FN1, FBLN1), were predominantly associated with pro-inflammatory processes, ECM deposition, and metabolic regulation. In contrast, downregulated proteins such as cytoskeletal proteins (VCL, TLN1), signaling molecules (SRC, RAP1B), and immune factors (HLA-A, FCN1, PSMB7) were mainly involved in cell adhesion impairment, inhibition of migration, and attenuation of immune responses.

Erosive OLP was characterized by the co-activation of coagulation and complement pathways (upregulation of C3 and FGA) and basement membrane stiffening (upregulation of COL6A1), contributing to mucosal barrier disruption. The non-erosive form primarily exhibited antibody gene alterations (upregulation of IGHV) and neural repair dysregulation (upregulation of THBS4 with downregulation of NCAM1), manifesting clinically as persistent white reticular lesions. These distinctions indicate that erosive OLP is driven by a thromboinflammatory microenvironment that facilitates tissue injury, whereas non-erosive OLP is associated with immune and neuroregulatory disturbances that maintain keratinization abnormalities. Notably, shared molecular targets such as CALCRL, FN1, and VCL may offer therapeutic relevance across OLP phenotypes.

GO enrichment analysis of differential serum exosome proteins revealed consistent enrichment across all groups in the extracellular region, extracellular space, and vesicle-related components. These findings support the hypothesis that exosomes function as vehicles for modulating the OLP microenvironment by targeted delivery of proteins such as complement components, ECM-related molecules, and signaling factors. In terms of molecular function, enrichment in protein binding, protein complex binding, and signal receptor binding across all groups suggests that these proteins participate in the formation of functional complexes (eg, immunological synapses and ECM networks), which may enhance pathological signaling cascades.

Biological process analysis demonstrated distinct patterns among the groups. In the disease group versus normal group comparison, enrichment was observed in processes related to cell adhesion and wound healing, indicating a disruption in mucosal barrier repair mechanisms driving ECM fibrosis. The non-erosive versus normal group comparison was enriched in immune system regulation and stress response pathways, indicating a persistent immune-inflammatory condition reflective of a chronic disease state. The erosive versus normal group exhibited enrichment in substance transport and localization regulation, potentially linked to impaired vesicle trafficking and delayed tissue regeneration.

Lastly, the comparison between non-erosive and erosive groups demonstrated enrichment in response to organic substances and oxidative stress, highlighting differences in the local metabolic microenvironment, such as lipid peroxidation, and variations in nociceptive signaling potentially mediated by calcium signaling imbalances. These findings collectively indicate that the progression of OLP subtypes involves dynamic remodeling of the tissue microenvironment mediated by exosome-transported differential proteins. The transition from non-erosive to erosive forms appears to follow a pathological trajectory marked by "immune suppression → metabolic dysfunction → compensatory reparative inflammation".

KEGG pathway enrichment analysis of serum exosome differential proteins across the four groups revealed three commonly enriched pathways: platelet activation, focal adhesion, and regulation of the actin cytoskeleton. These findings indicate that, irrespective of OLP subtype, coagulation disturbances, disruptions in cell-ECM interactions, and cytoskeletal remodeling are consistently implicated. This indicates that a pathological framework involving complement, coagulation, and cytoskeletal systems may represent the central pathogenic mechanism underlying OLP. Specifically, MAC activity and fibrin microthrombus formation (mediated by FGA and C3) likely contribute to basement membrane injury. Simultaneously, disrupted integrin-ECM signaling (involving FN1 and ITGB3) and actin cytoskeleton disintegration (TPM3 and CAPZA2) together drive the breakdown of the epithelial barrier. Notably, the complement and coagulation cascade pathways were significantly enriched in the disease, non-erosive, and erosive groups, but were absent in the comparison between non-erosive and erosive groups, indicating that the transition toward erosive OLP may coincide with reduced dominance of the coagulation system.

Subtype-specific pathway enrichment revealed additional distinctions. In the disease group, "proteoglycans in cancer" and "SNARE vesicular transport" pathways were significantly enriched, potentially reflecting abnormalities in ECM glycosaminoglycan metabolism and exosome secretion mechanisms, respectively. In the non-erosive group, enrichment in "antigen processing and presentation" and "leukocyte transendothelial migration" pathways implied a greater reliance on adaptive immune infiltration. The erosive group was uniquely enriched in the "renin-angiotensin system" and "neutrophil extracellular trap formation" pathways, indicating the contribution of angiotensin II-driven inflammation and NETosis-mediated tissue damage. In the non-erosive versus erosive comparison, novel enrichment of metabolism-related pathways was observed, including PPAR signaling and cholesterol metabolism. Inhibition of PPARγ, a central regulator of lipid metabolism, may result in energy deficiency during tissue repair, while disruptions in cholesterol metabolism may impair membrane integrity. Concurrent enrichment of the "intestinal immune network for IgA production" further implicated oral-gut mucosal immunity in the phenotypic transition. Collectively, these findings indicate the need for stage-specific therapeutic strategies. Targeting RAP1 and integrin signaling may stabilize epithelial adhesion in non-erosive OLP, while suppressing the PI3K-AKT-NETosis axis and regulating PPARγ activity may be more effective during erosive progression. Persistent complement-coagulation axis activation across all subtypes highlights a promising unified therapeutic target.

Protein-protein interaction network analysis of differential proteins between the disease and normal groups identified several key regulators of OLP pathophysiology, including FN1, ALB, ACTB, C3, APOA1, ITGB3, TLN1, ITGA2B, VCL, SRC, FLNA, ACTR2, MASP1, PLA2G7, DCTN2, YWHAB, CDC42, YWHAQ, RAP1B, and LTBP1. Here, FN1 emerged as the central hub protein, with the highest betweenness centrality, interacting with integrin receptors (ITGA2B

and ITGB3), focal adhesion mediator (VCL), and TGF-β anchor (LTBP1). Upregulation of FN1 promotes the formation of abnormal ECM fiber networks, while downregulation of ITGB3 and VCL disrupts integrin-actin signaling, ultimately contributing to epithelial-mesenchymal detachment, a fundamental mechanism in erosion formation. Furthermore, the complement-coagulation axis demonstrated positive feedback amplification. The lectin pathway initiator MASP1, which was upregulated, activates C3 convertase, facilitating C3 cleavage and MAC assembly. Simultaneously, upregulated phospholipase PLA2G7 hydrolyzes oxidized phospholipids to generate prothrombotic mediators, collectively promoting microvascular occlusion and basement membrane breakdown.

Within the cytoskeletal and tissue repair network, disorganization of actin structures (with downregulation of ACTB, FLNA, and ACTR2) and impairment of cellular migration signals were evident. Members of the 14-3-3 protein family (YWHAB and YWHAQ) sequestered phosphorylated SRC and CDC42, thereby inhibiting activation of RAP1B-mediated cell spreading, resulting in defective epithelial regeneration. This interaction map indicates a three-tier pathological cascade in OLP: FN1-integrin mechanical coupling dysfunction leads to epithelial-ECM separation; the MASP1-C3-PLA2G7 axis drives a thromboinflammatory cascade; and inactivation of SRC and CDC42 via 14-3-3 proteins impairs reparative function. The hub proteins FN1 and C3 represent central nodes in this network and may serve as optimal candidates for future targeted interventions.

This study proposes that the complement-coagulation-ECM axis forms the pathological framework of OLP: complement overactivation (C3↑) and antigen processing defects (PSMB7↓/FCN1↓) create an autoimmune cycle, which, through HLA-DRB1 overpresentation of self-antigens, drives CD4+ T cell-mediated chronic inflammation and basal cell apoptosis. Simultaneously, subtype-specific tissue remodeling manifests as accelerated collagen cross-linking by the FN1-THBS4 complex in non-erosive types, forming white stripe lesions, while the KLKB1-SERPINA10 axis in erosive types activates thrombin and inhibits fibrinolysis, inducing microthrombosis and degrading the COL6A1 basement membrane structure, ultimately leading to epithelial detachment. At the microenvironmental level, the transition from non-erosive to erosive types reflects metabolic-immune compensatory reprogramming—upregulation of SLC25A6/LPL provides repair energy, downregulation of IGHV weakens autoimmune attacks, but NCAM1 deficiency disrupts neurogenic anti-inflammatory signals, trapping the lesion area in a vicious cycle of "high-energy repair-inflammation resolution impairment." This framework not only elucidates the dynamic coupling mechanism of immune dysregulation, matrix dissolution, and metabolic adaptation but also proposes an innovative therapeutic strategy targeting the C3/FN1 core nodes in conjunction with the KLKB1-SLC25A6 pathway regulation.

Limitations

This study has several limitations that should be considered when interpreting the results. Firstly, the relatively small sample size may reduce the statistical power to detect smaller effect sizes and limit the generalizability of our findings to broader populations. Secondly, although stringent purification protocols were employed (combining size-exclusion chromatography and validation via TSG101/ALIX positivity and Calnexin negativity), potential co-isolation of non-exosomal components inherent to current isolation techniques cannot be entirely ruled out. This may introduce confounding factors in downstream omics analyses; thus, results should be interpreted with this caveat in mind. Thirdly, variability in exosome isolation and characterization methods across laboratories remains a recognized challenge. Despite adherence to MISEV2018 guidelines and strict protocol standardization, inherent technical variability could affect quantitative comparisons between samples. Finally, our bioinformatics analyses, while utilizing established databases and pipelines, are subject to limitations. These include dependence on underlying statistical assumptions (eg, normality, homogeneity of variance), incomplete functional annotations in reference databases, and the impact of selected significance thresholds (eg, p-value/FDR cutoff), which may influence the accuracy of differential expression and pathway enrichment results. Despite these limitations, our findings provide valuable preliminary evidence. Future studies with larger cohorts, refined isolation/characterization techniques, mechanistic studies using in vitro/ex vivo models and experimental validation of bioinformatic predictions are warranted to confirm and extend these observations.

Conclusion

High-purity serum exosomes were successfully isolated using SEC in combination with NTA, TEM, and WB, providing a reliable methodological basis for subsequent omics-based investigations.

Distinctive characteristics of the differential protein profiles were observed. Regarding common features across OLP subtypes, all groups demonstrated significant enrichment of complement and coagulation cascade pathways (including C3 and FGA), dysregulation of cell adhesion (evidenced by FN1 and VCL downregulation), and immune abnormalities (with HLA-DRB1 upregulation and HLA-A downregulation). In terms of subtype-specific features, the erosive subtype was marked by coagulation and fibrinolytic imbalance (with KLKB1 and SERPINA10 upregulation) and basement membrane damage (COL6A1 upregulation), whereas the non-erosive subtype demonstrated pronounced autoantibody activation (IGHV upregulation) and impaired neural repair (NCAM1 downregulation).

Key pathogenic mechanisms were further delineated. Disruption of fibronectin-integrin (FN1-ITGB3) signaling contributed to epithelial-extracellular matrix separation, facilitating erosion formation. The MASP1-C3-PLA2G7 axis promoted a thromboinflammatory microenvironment, which, in conjunction with inactivation of SRC and CDC42 mediated by 14-3-3 family proteins (such as YWHAB), impeded tissue repair processes. Collectively, the complement-coagulation cascade and cytoskeletal remodeling were identified as integral components of a unified pathological framework underlying OLP.

Identified serum exosome proteins, particularly FN1 and C3, and their associated networks represent highly promising non-invasive diagnostic biomarkers. Critically, these findings provide a strong rationale for developing targeted therapies, including complement inhibitors (eg, anti-C3) and strategies promoting epithelial regeneration.

In essence, this work defines the critical exosomal protein landscape of OLP, elucidates novel subtype-specific mechanisms within a unified pathological framework of thromboinflammation and cytoskeletal dysfunction, and directly points the way towards improved diagnosis and mechanism-based therapeutics.

Abbreviation

OLP, Oral lichen planus; WB, Western blotting; NTA, Nanoparticle tracking analysis; TEM, Transmission electron microscopy; GO, Gene Ontology; KEGG, Kyoto Encyclopedia of Genes and Genomes; PPI, Protein-Protein Interaction; BP, Biological Process; CC, Cellular Component; MF, Molecular Function; MVB, multivesicular body; SEC, Size Exclusion Chromatography; BC, Betweeness Centrality; MS, Mass Spectrometry; ECM, extracellular matrix.

Data Sharing Statement

All data generated or analysed during this study are included in this article. Further enquiries can be directed to the corresponding author.

Ethics Approval and Consent to Participate

This study was conducted in accordance with the declaration of Helsinki. Informed consent was obtained from all participants prior to inclusion, and ethical approval was granted by the Ethics Committee of Fujian Medical University Union Hospital (approval no. 2023KY064).

Acknowledgments

We would like to acknowledge the hard and dedicated work of all the staff that implemented the intervention and evaluation components of the study.

Funding

1)Provincial Financial Subsidy Funds for Health in Fujian (2022CZ005): Wei-Qun Guan; 2)Joint Funds for the Innovation of Science and Technology, Fujian Province (2021Y9063): Xue-Ying Wang.

Disclosure

The authors declare that they have no competing interests in this work.

References

1. Netto JNS, Pires FR, Costa KHA, Fischer RG. Clinical features of oral lichen planus and oral lichenoid lesions: an oral pathologist's perspective. *Braz Dent J*. 2022;33(3):67–73. doi:10.1590/0103-6440202204426
2. Nukaly HY, Halawani IR, Alghamdi SMS, et al. Oral lichen planus: a narrative review navigating etiologies, clinical manifestations, diagnostics, and therapeutic approaches. *J Clin Med*. 2024;13(17):5280. doi:10.3390/jcm13175280
3. C K-DP, Ramos-García P, Má G-M. A molecular hypothesis on malignant transformation of oral lichen planus: a systematic review and meta-analysis of cancer hallmarks expression in this oral potentially malignant disorder. *Cancers*. 2024;16(15):2614. doi:10.3390/cancers16152614
4. Saeed S, Choudhury P, Ahmad SA, et al. Vitamin D in the treatment of oral lichen planus: a systematic review. *Biomedicines*. 2022;10(11):2964. doi:10.3390/biomedicines10112964
5. Kim TJ, Kim YG, Jung W, et al. Non-coding RNAs as potential targets for diagnosis and treatment of oral lichen planus: a narrative review. *Biomolecules*. 2023;13(11):1646. doi:10.3390/biom13111646
6. Tenório JR, de Camargo AR, Lemos C, Ortega KL. Oral lichen planus and HCV infection. *Autops Case Rep*. 2020;10(4):e2020210. doi:10.4322/acr.2020.210
7. Ciesielska A, Ossowska A, Kusiak A, Grzybowska ME. Changes in the oral cavity in menopausal women-a narrative review. *Int J Environ Res Public Health*. 2021;19(1):253. doi:10.3390/ijerph19010253
8. Rassol HJ, Zaidan TF. Immunohistochemical expression of T-cell subsets (CD4 and CD8) in oral lichen planus. *Pan Afr Med J*. 2023;45:147. doi:10.11604/pamj.2023.45.147.38629
9. Rotaru D, Chisnoiu R, Picos AM, Chisnoiu A, Picos A. Treatment trends in oral lichen planus and oral lichenoid lesions (Review). *Exp Ther Med*. 2020;20(6):198. doi:10.3892/etm.2020.9328
10. Xu S, Zhang Y, Zheng Z, Sun J, Wei Y, Ding G. Mesenchymal stem cells and their extracellular vesicles in bone and joint diseases: targeting the NLRP3 inflammasome. *Hum Cell*. 2024;37(5):1276–1289. doi:10.1007/s13577-024-01101-x
11. Lu F, Ye M, Shen Y, et al. Hypoxic tumor-derived exosomal miR-4488 induces macrophage M2 polarization to promote liver metastasis of pancreatic neuroendocrine neoplasm through RTN3/FABP5-mediated fatty acid oxidation. *Int J Biol Sci*. 2024;20(8):3201–3218. doi:10.7150/ijbs.96831
12. Peng Y, Li Y, Yang Y, Shi T, Luan Y, Yin C. Exosome and virus infection. *Front Immunol*. 2023;14:1154217. doi:10.3389/fimmu.2023.1154217
13. Liu M, Wen Z, Zhang T, Zhang L, Liu X, Wang M. The role of exosomal molecular cargo in exosome biogenesis and disease diagnosis. *Front Immunol*. 2024;15:1417758. doi: 10.3389/fimmu.2024.1417758
14. Peng Q, Zhang J, Zhou G. Differentially circulating exosomal microRNAs expression profiling in oral lichen planus. *Am J Transl Res*. 2018;10(9):2848–2858.
15. Ding M, Wang X, Wang C, et al. Distinct expression profile of HCMV encoded miRNAs in plasma from oral lichen planus patients. *J Transl Med*. 2017;15(1):133. doi:10.1186/s12967-017-1222-8
16. Byun JS, Hong SH, Choi JK, Jung JK, Lee HJ. Diagnostic profiling of salivary exosomal microRNAs in oral lichen planus patients. *Oral Dis*. 2015;21(8):987–993. doi:10.1111/odi.12374
17. Agrawal H, Patil RK, Singh V, et al. Salivary and serum estrogen level assessment in oral lichen planus patients and its correlative analysis with OLP and stress. *J Family Med Prim Care*. 2024;13(5):1998–2005. doi:10.4103/jfmpc.jfmpc_1332_23
18. Bao ZX, Yang XW, Shi J, Wang YF. The profile of hematinic deficiencies in patients with oral lichen planus: a case-control study. *BMC Oral Health*. 2020;20(1):252. doi:10.1186/s12903-020-01229-w
19. Wang Z, Zhou X, Kong Q, et al. Extracellular vesicle preparation and analysis: a state-of-the-art review. *Adv Sci*. 2024;11(30):e2401069. doi:10.1002/advs.202401069
20. Duong VA, Lee H. Bottom-up proteomics: advancements in sample preparation. *Int J Mol Sci*. 2023;24(6):5350. doi:10.3390/ijms24065350
21. Abuhamad AY, Mohamad Zamberi NN, Vanharanta S, Mohd Yusuf SNH, Mohtar MA, Syafruddin SE. Cancer cell-derived PDGFB stimulates mTORC1 activation in renal carcinoma. *Int J Mol Sci*. 2023;24(7):6447. doi:10.3390/ijms24076447
22. El-Howati A, Thornhill MH, Colley HE, Murdoch C. Immune mechanisms in oral lichen planus. *Oral Dis*. 2023;29(4):1400–1415. doi:10.1111/odi.14142
23. Lester DK, Burton C, Gardner A, et al. Fucosylation of HLA-DRB1 regulates CD4+ T cell-mediated anti-melanoma immunity and enhances immunotherapy efficacy. *Nat Cancer*. 2023;4(2):222–239. doi:10.1038/s43018-022-00506-7
24. Zhang L, Cui Y, Mei J, Zhang Z, Zhang P. Exploring cellular diversity in lung adenocarcinoma epithelium: advancing prognostic methods and immunotherapeutic strategies. *Cell Prolif*. 2024;57(11):e13703. doi:10.1111/cpr.13703
25. Padyukov L. Genetics of rheumatoid arthritis. *Semin Immunopathol*. 2022;44(1):47–62. doi:10.1007/s00281-022-00912-0
26. Meyer BJ, Kunz N, Seki S, et al. Immunologic and genetic contributors to CD46-dependent immune dysregulation. *J Clin Immunol*. 2023;43(8):1840–1856. doi:10.1007/s10875-023-01547-y
27. Zhang Z, Geng X, Yin M, et al. Unveiling ficolins: diagnostic and prognostic biomarkers linked to the tumor microenvironment in lung cancer. *World J Surg Oncol*. 2024;22(1):273. doi:10.1186/s12957-024-03558-4
28. Di Nubila A, Dilella G, Simone R, Barbieri SS. Vascular extracellular matrix in atherosclerosis. *Int J Mol Sci*. 2024;25(22):12017. doi:10.3390/ijms252212017
29. Kögl T, Chang HF, Staniek J, et al. Patients and mice with deficiency in the SNARE protein SYNTAXIN-11 have a secondary B cell defect. *J Exp Med*. 2024;221(7):e20221122. doi:10.1084/jem.20221122
30. Zarantonello A, Revel M, Grunenwald A, Roumenina LT. C3-dependent effector functions of complement. *Immunol Rev*. 2023;313(1):120–138. doi:10.1111/imr.13147
31. Moellmer SA, Puy C, McCarty OJT. Biology of factor XI. *Blood*. 2024;143(15):1445–1454. doi:10.1182/blood.2023020719
32. Li H, Zhang Z, Qiu Y, et al. Proteome-wide mendelian randomization identifies causal plasma proteins in venous thromboembolism development. *J Hum Genet*. 2023;68(12):805–812. doi:10.1038/s10038-023-01186-6
33. Zeng H, Lan B, Li B, et al. The role and mechanism of thrombospondin-4 in pulmonary arterial hypertension associated with congenital heart disease. *Respir Res*. 2024;25(1):313. doi:10.1186/s12931-024-02932-w